Proceedings of the ASME 2015 International Design Engineering Technical Conferences & Computers and Information in Engineering Conference

IDETC/CIE 2015

August 2 – August 5, 2015, Boston, MA, USA

DETC2015-46356

TOWARDS ASSEMBLY-FREE METHODS FOR ADDITIVE MANUFACTURING SIMULATION

Anirudh Krishnakumar
Graduate Student
Department of Mechanical Engineering
UW-Madison, Madison, Wisconsin 53706, USA
Email: krishankumaranirudh@gmail.com

Krishnan Suresh
Associate Professor
Department of Mechanical Engineering
UW-Madison, Madison, Wisconsin 53706, USA
Email: suresh@engr.wisc.edu

Aaditya Chandrasekar
Undergraduate Student
Department of Mechanical Engineering
SRM University, Kattankulathur,
Tamil Nadu 603203, India
Email: cs.aaditya@gmail.com

ABSTRACT

There is significant interest today in the finite element simulation of various Additive Manufacturing (AM) processes. AM simulation is time-dependent, inherently non-linear, and involves multiple physics. In addition, repeated meshing and insertion of new elements during material deposition can pose significant implementation challenges.

Currently, AM simulation is handled either through a 'quiet' approach or an 'inactive' approach. In the quiet approach, all finite elements within the workspace are assembled into the global stiffness matrix, and the elements yet to be deposited are assigned 'void' material properties. In the inactive approach, only the elements that have been deposited are assembled into the global stiffness matrix. The advantages and disadvantages of the two methods are well documented.

In this paper, we propose a voxel-based, assembly-free framework for AM simulation. This framework presents several advantages including. (1) The workspace is meshed only once at the start of the simulation, (2) addition and deletion of elements is trivial, (3) reduced memory requirement as the global stiffness matrix is never assembled and (4) the underlying linear systems of equations can be solved efficiently through assembly-free methods. We demonstrate the framework here by simulating transient non-linear thermal behaviour of a laser deposition process, with material deposition.

INTRODUCTION

Additive Manufacturing (AM), sometimes referred to as 3D-printing, captures various manufacturing processes that fabricate components layer-by-layer, directly from a digital part description, such as a Stereolithography (STL) description [1].

AM has received significant attention lately due to its inherent advantages [2] including: (1) ability to handle complex geometry, (2) direct prototyping with minimal setup time, (3) reduced need for skilled labor, and (4) reduced material wastage. For example, consider the part in Figure 1; while one can certainly make this part through conventional subtractive processes, it will lead to significant wastage. AM, on the other hand, will minimize wastage.

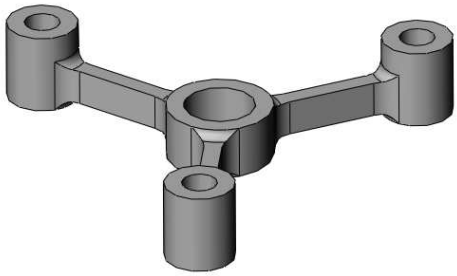

Figure 1: ADDITIVE MANUFACTURING OF THIS ILLUSTRATIVE PART WILL LEAD TO MINIMAL WASTAGE.

There are many types of AM processes [3], [4]–[7] based on the choice of stock material, and bonding method. The stock material can be in the form of powder bed, powder jet, wire feed, or material extrusion, while the material bonding can be carried out by applying a liquid bonding agent, direct solidification, or by the application of thermal energy in the form of lasers or electron beams.

In this paper, we focus on the laser engineering net shaping (LENS) method which uses powder jet nozzles to feed the stock material, and lasers to induce melting and bonding. LENS was developed at the Sandia National Laboratories, and is currently commercialized through Optomec Design Company. The most

commonly used materials in LENS include titanium alloys (Ti6Al4V), stainless steel alloys, aluminum, copper and nickel alloys. The laser used in the method is usually Nd-Yag [8].

In the LENS process, one starts with a substrate. A high-powered laser beam is then used to create a molten pool into which the metallic powder is simultaneously fed. The beam is moved along with the powder feed jet to trace out the first slice of the layer of the part, as shown in Figure 2. The process is repeated layer by layer, until the part is completed.

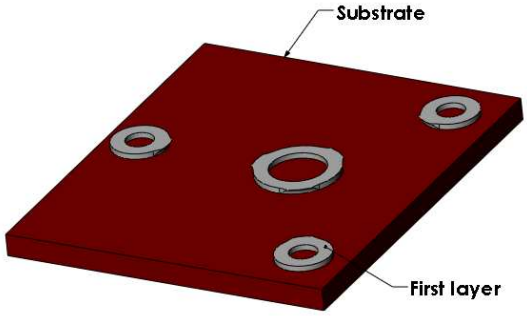

Figure 2: A SCHEMATIC REPRESENTATION OF THE SUBSTRATE WITH THE FIRST LAYER OF METAL DEPOSITION.

The transient thermal behavior of the above process largely determines the solidification rate, void formation and residual stresses, which in turn determine the final quality, microstructure and reliability of the manufactured part [9], [10].

A good understanding of the thermal behavior and its dependency on the process parameters (feed-rate, laser energy, and thermal boundary conditions) are therefore of paramount importance [11]. The most common method for simulating such processes is transient finite element analysis.

FINITE ELEMENT SIMULATION

Mathematical Model

The AM process can largely be modeled via the energy equation [1], [11]:

$$\rho\frac{\partial h}{\partial t}+\frac{\partial(\rho u_i h)}{\partial x_i}=\begin{bmatrix}\dfrac{\partial}{\partial x_i}\left(\dfrac{k}{c_p}\dfrac{\partial E}{\partial x_i}\right)-\rho\dfrac{\partial(\Delta H)}{\partial t}-\\ \dfrac{\partial(u_i\Delta H)}{\partial x_i}+Q\end{bmatrix} \tag{2.1}$$

Where

E : sensible heat (c_pT)
k : thermal conductivity
c_p : specific heat
Q : internal energy source
ΔH : latent heat content
ρ : density
u : velocity of conserved mass
x_i : x,y,z coordinates

(2.2)

From the energy equation, we extract just the transient thermal finite element governing equation, by ignoring (for the purpose of this paper) the phase change and the fluid flow [12], [13]. Now, the Equation (2.1) simplifies to:

$$\frac{\partial}{\partial x_i}(k_i\frac{\partial T}{\partial x_i})+Q=\rho c_p\frac{dT}{dt} \tag{2.3}$$

Boundary conditions include a combination of Dirichlet (fixed temperature), heat source, convective, and radiative conditions. A detailed description can be found in [14]. Through the classic finite element based Galerkin formulation [15], the governing equation and boundary conditions can be collapsed into:

$$\begin{bmatrix}\int_\Omega \rho c_p N_i N_j\dfrac{dT_j}{dt}d\Omega+\int_\Omega k_{ij}.\dfrac{\partial N_i}{\partial x_i}\dfrac{\partial N_j}{\partial x_j}T_j d\Omega\\ -\int_\Omega N_i Q\,d\Omega\\ +\int_\Gamma N_i\left[-q_a+h(T-T_0)+\varepsilon\sigma(T^4-T_0^4)\right]d\Gamma\end{bmatrix}=0 \tag{2.4}$$

Where

N : classic finite element shape functions
q_a : applied heat flux (-ve due to sign convention)
h : heat transfer coefficient($\mathrm{W/m^2K}$)
ε : emissivity [0,1]
σ : stefan boltzmann constant($5.67*10^{-8}\mathrm{W/m^2K^4}$)

If the non-linear radiative boundary condition is expressed as:

$$(T^4-T_0^4)=(T^2+T_0^2)(T+T_0)(T-T_0) \tag{2.5}$$

Then, the finite element discretization, Equation (2.4), together with Equation (2.5), can be reduced to:

$$[C]\{\dot{T}\}+[K]\{T\}=\{F\} \tag{2.6}$$

Where

$$[C]=\int_\Omega \rho c_p[N]^T[N]d\Omega \tag{2.7}$$

$$[K]=\begin{bmatrix}\int_\Omega[B]^T[D][B]d\Omega+\int_\Gamma h[N]^T[N]\,d\Gamma+\\ \int_\Gamma \varepsilon\sigma(T^2+T^2{}_0)(T+T_0)[N]^T[N]\,d\Gamma\end{bmatrix} \tag{2.8}$$

$$\{F\}=\begin{bmatrix}\int_\Omega[N]Q\,d\Omega+\int_{\Gamma_q}q_a[N]d\Gamma+\int_\Gamma hT_0[N]d\Gamma\\ +\int_\Gamma \varepsilon\sigma(T^2+T_0^2)(T+T_0)T_0[N]d\Gamma\end{bmatrix} \tag{2.9}$$

$$[B]=\nabla[\mathrm{N}] \tag{2.10}$$

The laser heat source, can be treated as a volumetric internal energy source Q in Equation (2.9) and is typically modeled using a double ellipsoidal model [9], [16]

$$Q=\frac{6\sqrt{3}\eta Pf\exp\left[-\frac{3x^2}{a^2}-\frac{3y^2}{b^2}-\frac{3(z+v_wt)^2}{c^2}\right]}{abc\pi\sqrt{\pi}} \tag{2.11}$$

where

P : laser power(W)
η : process efficiency
f : scaling factor
a : transverse depth(m)
b : melt pool depth(m)
c : longitudinal ellipsoid axis(m)
t : time(s)
v_w : heat source velocity(m/s) (2.12)

The advantage of using a double ellipsoidal is that the front gradient can be made steeper than the rear, replicating the laser.

Time Stepping

To solve Equation (2.6), we rely on the Newmark Beta method for time-stepping [17], where:

$$\{T\}_{n+1} = \{T\}_n + \Delta t\left\{(1-\beta)\dot{T}_n + \beta\dot{T}_{n+1}\right\} \tag{2.13}$$

By multiplying Equation (2.6) with (1-β) at time step 'n' and β at time step 'n+1', and then, adding the two will result in:

$$\left(\frac{1}{\Delta t}[C]+\beta[K]_{n+1}\right)\{T_{n+1}\} = \left(\frac{1}{\Delta t}[C]-(1-\beta)[K]_n\right)\{T_n\}+(1-\beta)\{F\}_n+(\beta)\{F\}_{n+1} \tag{2.14}$$

Here the heat capacity matrix [C] is independent of time and temperature. This can be expressed in the form:

$$[K_{eff}]\{T_{n+1}\} = \{F_{eff}\}_{n+1} \tag{2.15}$$

where:

$$[K_{eff}] = \left(\frac{1}{\Delta t}[C]+\beta[K]\right) \tag{2.16}$$

$$\{F_{eff}\}_{n+1} = \left[\begin{array}{l}\left(\frac{1}{\Delta t}[C]-(1-\beta)[K]\right)\{T_n\}+\\ (1-\beta)\{F\}_n+(\beta)\{F\}_{n+1}\end{array}\right] \tag{2.17}$$

Observe that the stiffness matrix is temperature dependent due to the radiative term, and dependency of the material properties on the temperature. Thus, at every time step one must solve a non-linear set of equations. Here we use $\beta = 1$ to ensure unconditional stability. In other words:

$$[K_{eff}] = \left(\frac{1}{\Delta t}[C]+[K]\right) \tag{2.18}$$

$$\{F_{eff}\}_{n+1} = \frac{1}{\Delta t}[C]\{T_n\}+\{F\}_{n+1} \tag{2.19}$$

Inherent Challenges

In the LENS process, the temperature changes are large and very rapid (for example, the temperature can increase from 20˚C to 1670˚C in milliseconds [14]) with large temperature gradients. This entails small time steps, and a fine resolution of the geometry. Adaptive mesh techniques are often used [16], with fine discretization near the heat source and on the top few layers. However, as the laser traverses, and as the material is added to the top layer, constant re-meshing is required.

Finally, to account for material deposition, two methods, namely, quiet-element and inactive-element methods are currently used [16].

In the quiet approach, all finite elements within the workspace are assembled into the global stiffness matrix, but the elements yet to be deposited are assigned 'void' material properties. They are later assigned appropriate material properties, as and when needed. The method uses a constant mesh, and is simple to implement, but the incorrect selection of scaling factors can lead to ill-conditioning of the Jacobian.

The inactive method uses an evolving mesh, and includes only the active elements for simulation. This leads to high simulation speeds, especially during the initial stages. However, constant re-meshing and re-formulation of the finite element equation can be time consuming and difficult to implement. A hybrid technique has been used in [16].

To overcome these challenges, we propose a voxel-based, assembly-free method which does not require the matrices to be assembled. This method can be used to deal with the various nonlinearities of the system. This method can also effectively model the material deposition and has several advantages over the quiet and inactive methods.

PROPOSED METHOD

Voxelization

Voxelization is a special form of finite element discretization where all elements are identical (hexahedral elements). For example, Figure 3 illustrates the voxel mesh of the geometry in Figure 2. The most important advantage of voxelization is its robustness; voxelization rarely fails unlike classic meshing. In addition, voxelization significantly reduces memory foot-print since the element stiffness matrices are all identical; this directly translates into increased speed of analysis.

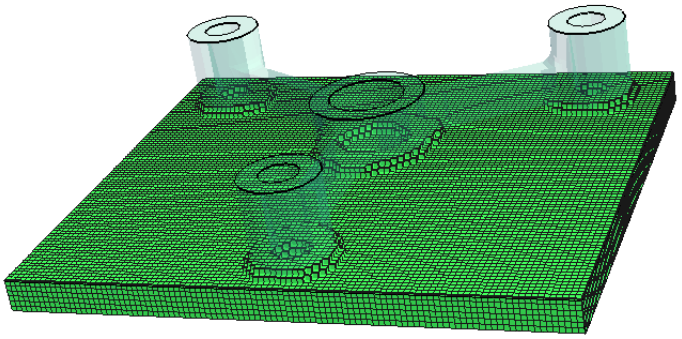

Figure 3: UNIFORM VOXELIZATION OF GEOMETRY FROM Figure 2.

Voxels have been used in additive manufacturing, for example, to find effective mechanical properties [18]. In this paper, voxels are used as a computational unit. In the present approach, the entire workspace is discretized once, at the beginning of the simulation (see Figure 4). As with the inactive element method, the elements to be deposited are inactive. However, unlike the inactive approach, the global stiffness

matrix is never assembled. The challenges associated with 'void' material assignment are overcome through assembly-free analysis.

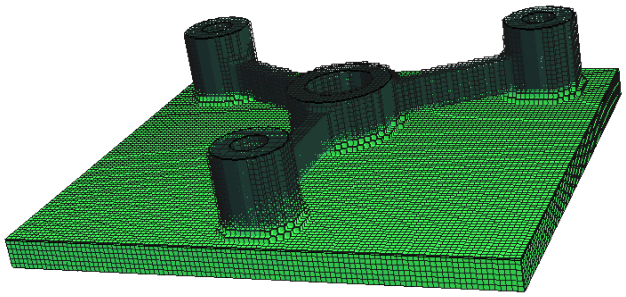

Figure 4: ELEMENTS TO BE DEPOSITED ARE INACTIVE.

Assembly Free Analysis

Assembly-free finite element analysis was proposed by Hughes and others in 1983 [19]. In recent years, it has resurfaced due to the surge in fine-grain parallelization. The basic concept used in the analysis is that the stiffness matrix is never assembled; instead, matrix operations are performed in an assembly-free elemental level [20], [21]. For example, the typical Sparse Matrix Vector Multiplication (SpMV) is typically implemented by first assembling the element stiffness matrices as follows:

$$\{Kx\} = \left(\sum_e [K_e] \right) \{x\} \tag{3.1}$$

In an assembly free method, this is implemented by first carrying out the multiplications at the element level, and then assembling the results:

$$\{Kx\} = \sum_e \left([K_e]\{x_e\} \right) \tag{3.2}$$

Assembly free analysis is not advantageous when elements are distinct from each other (as in a classic finite element mesh). However, with voxelization, since all elements are identical, only one elemental 8*8 stiffness matrix needs to be stored, and Equation (3.2) can be executed rapidly, with reduced memory footprint.

In AM simulation, as elements are deposited, introducing them into the computation is also trivial. An additional element (with identical stiffness matrix) needs to be inserted while evaluating Equation (3.2). Similarly, the boundary conditions can be updated.

The SpMV in Equation (3.2) serves as the backbone of the classic Conjugate Gradient (CG) solver [20], [21]. For the thermal problem, preconditioners are not needed since the stiffness matrix is typically well conditioned.

In the current context of SpMV, the matrix is the effective stiffness matrix given by Equation (2.18). It consists of the C matrix and the stiffness matrix term *K* given by Equation (2.8). The C matrix can easily be treated in an assembly-free manner using a single copy of an element damping matrix. The *K* matrix can be broken up into the following 3 matrices:

$$[K] = [K_D] + [K_H] + [K_R]$$

where:

$$[K_D] = \int_\Omega [B]^T [D][B] d\Omega \tag{3.3}$$

$$[K_H] = \int_\Gamma h[N]^T [N]\, d\Gamma$$

$$[K_R] = \int_\Gamma \varepsilon\sigma (T^2 + T^2{}_0)(T + T_0)[N]^T [N]\, d\Gamma$$

The first term can be treated in an assembly-free manner using a single copy of an element stiffness matrix. However, for the convection and radiation matrices in Equation (3.3), since the integral is over the boundary, up to six different element stiffness matrices may have to be stored (to account for six different faces of a voxel). To accelerate computations, these two matrices are diagonalized here; this is analogous to the diagonalization (lumping) of the mass matrices [17]. The effective force vector given by Equation (2.19) is easy to evaluate in an assembly free manner.

Now consider the solution of the linear equation in Equation (2.15). This equation must be solved at each time-step. Since this is a non-linear equation, we rely on the iterative Newton Raphson method [22]. The T^0_{n+1} is obtained from the CG solver, and this is used to calculate the F^0_{eff}. The residual for the Newton Raphson process is then defined as:

$$\left\{R^i\right\} = [K^i_{n+1}]\left\{T^i_{n+1}\right\} - \left\{F^i_{eff}\right\}_{n+1} \tag{3.4}$$

The superscripts denote the iteration number of the Newton Raphson process. The subscripts denotes the current time step for which the temperature is required. One can now show that the tangent matrix used in the Newton Raphson process is given by:

$$[J^i] = \frac{\partial\{R^i\}}{\partial\{T\}} = [K_D] + [K_H] + 4[G_R]\{\{T^i_{n+1}\}^\wedge 3\}$$

where (3.5)

$$[G_R] = \int_\Gamma \varepsilon\sigma [N]^T [N]\, d\Gamma$$

Using the methodology described above, the Jacobian can be computed in an assembly free mmaner, followed by an assembly free update the temperature:

$$T^{i+1}_{n+1} = T^i_{n+1} - [J]^{-1}[R] \tag{3.6}$$

VERIFICATION STUDIES

The assembly-free, voxel-based method was tested and verified for a few steady state and transient thermal examples as follows. All FEA simulations were performed with an Intel(R) Core™ i5-3570 CPU processor with 8.00 GB RAM and a Windows 7 Operating System.

The results and speeds were then compared with ANSYS and SolidWorks on the same machine, with the same convergence criteria. All ANSYS and SolidWorks models were pre-meshed and only the time taken to solve the FEA problem was compared. Conjugate gradient iterative solvers were used in the present study. The CPU time taken for solving is obtained from

the Ansys and SolidWorks report, and is compared with the Voxel Based method.

Block Geometry: Effect of Diagonalization

The block in Figure 5 is of dimension 6m X 3m X 11m, and is made of Titanium with conductivity K=19.9W/mK, and boundary conditions as shown: fixed temperature on one-side, heat flux on the other, while all other faces are subject to surface losses through convection and radiation with h = 30W/m^{2}K and emissivity of ε = 0.6; the ambient temperature being T_0= 293K.

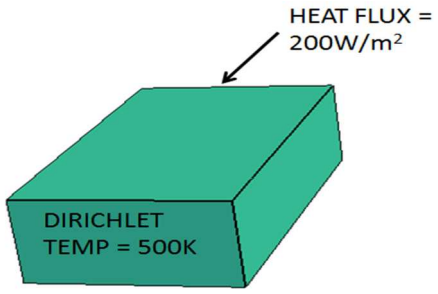

Figure 5: SIMPLE BLOCK PROBLEM.

Since the geometry is a simple block, there is no error due to voxelization. For about 2000 elements, ANSYS predicts a minimum temperature of 292.18K and a maximum temperature of 500K, SolidWorks predicts 292.13 and 500, and the proposed method predicts 292.16 and 500. A variety of such problems were solved and results compared. The proposed method yielded results within 0.02% of commercial implementations, suggesting that the error due to diagonalization is not significant, and may be negligible compared to unavoidable finite element discretization errors.

Curved Geometry: Effect of Voxel Mesh

Next, we will consider errors due to voxelization, using the part illustrated in Figure 6 that exhibit curved surfaces. The material is Alloy Steel with conductivity K=50W/mK; the boundary conditions are as illustrated: fixed temp of 300K on the left face, a convection boundary condition(C) with h = 100W/m^{2}K and a medium temperature of 423K on the inner cylindrical surface, and a radiation boundary condition, with ε = 0.4 and ambient temperature of 273K everywhere else.

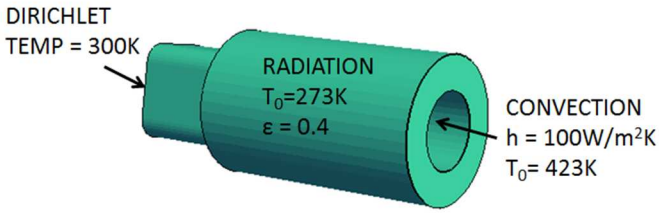

Figure 6: CURVED SURFACE GEOMETRY.

The part was discretized using 38000 voxel elements in our method, while a conforming tetrahedral mesh with the same number of elements was used both in ANSYS and SolidWorks. The temperature predictions from our method were within 0.14% of commercial implementations; the temperature distributions are illustrated in Figure 7.

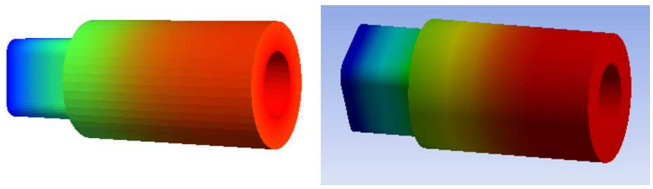

Figure 7: THERMAL DISTRIBUTION USING: (A) PROPOSED METHOD AND (b) ANSYS.

Further, Figure 8 illustrates the percentage deviation as a function of the number of elements. This is the typical deviation we have observed for curved geometry.

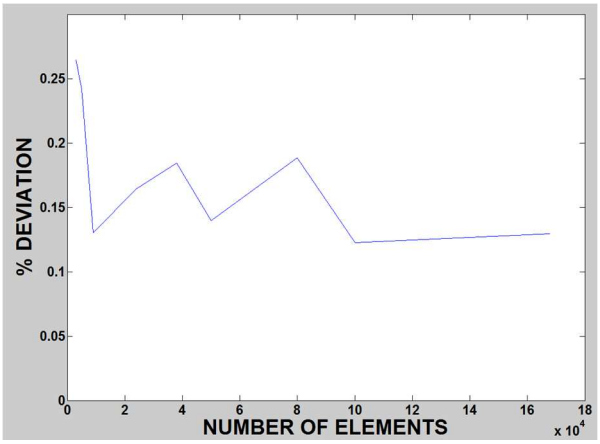

Figure 8: PERCENT DEVIATION VS NUMBER OF ELEMENTS.

For the above problem, Figure 9 illustrates the computing times as a function of the number of elements.

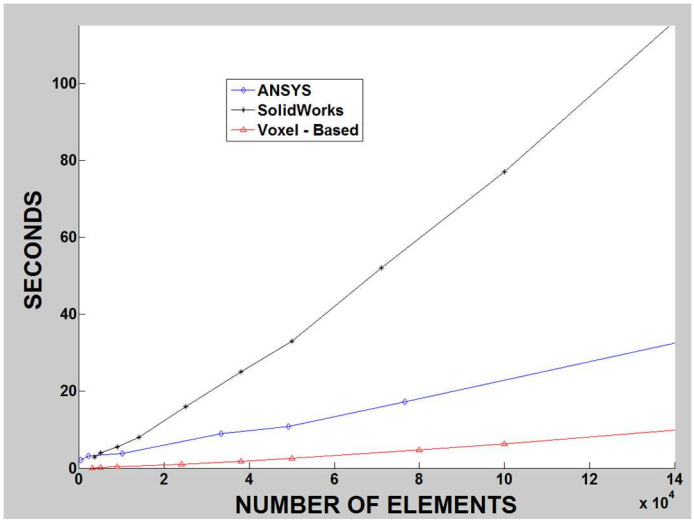

Figure 9: COMPUTING TIME VS NUMBER OF ELEMENTS.

Radiative Fin: Complex Geometry

An implicit advantage of voxelization is that complex geometry can be handled with ease. Figure 10 illustrates a radiative fin made of Copper, with K = 390W/mK, that is 7m long with an elliptical cross section and circular fins. Steam at 373K flows

inside (h = 10000W/m^{2}K), with heat dissipated from the fins (h = 35 W/m^{2}K, T_0 = 298K, emissivity = 0.03).

For a mesh with 80000 elements, the predicted temperature using our method was 362.44K (min) and 372.77K (max); see Figure 10b. These results deviated from commercial implementations by 0.02%. The solution time using our method was 6.5s, compared to 16s with ANSYS and 45s with SolidWorks.

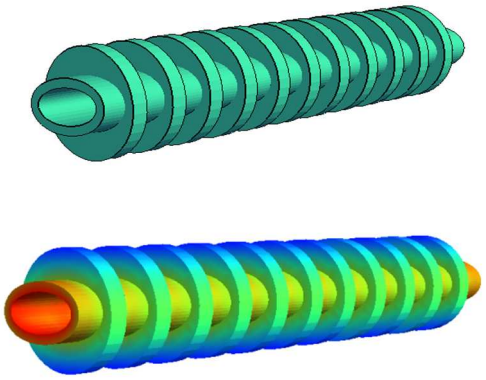

Figure 10: RADIATIVE FIN PROBLEM: (A) GEOMETRY, AND (B) TEMPERATURE DISTRIBUTION.

Transient Analysis

In this experiment, we will carry out a transient analysis on the geometry used in Section 4.2. The boundary conditions are as before, with the initial temperature of the body set to 298K. A mesh of 38,000 elements was used as before. The transient maximum temperature plots are illustrated in Figure 11.

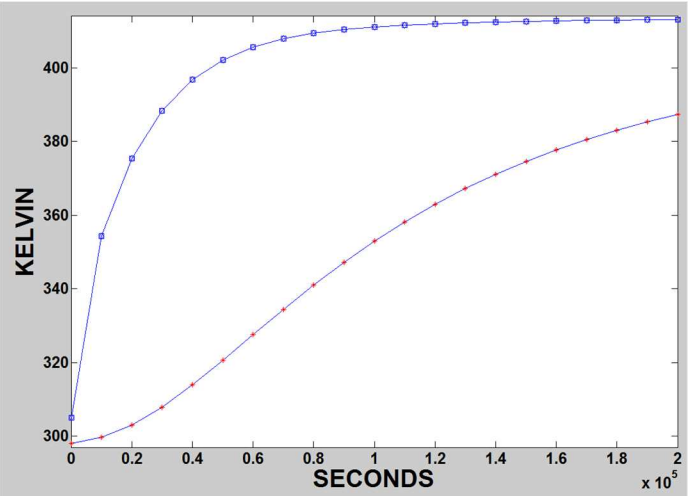

(a) PROPOSED VOXEL BASED METHOD.

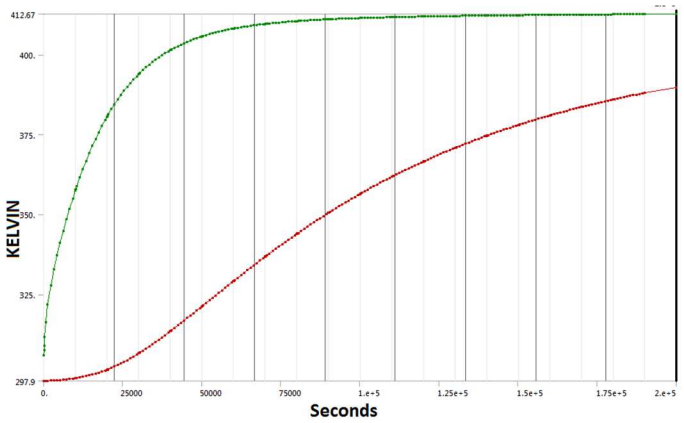

(b) ANSYS.

Figure 11: VARIATION OF TEMPERATURE OVER TIME.

The deviation of the proposed method from ANSYS was less than 0.133 percent, while the time taken by the proposed method was 585s compared to 3092s by ANSYS.

CASE STUDY

In this section, we will simulate the AM process of the part shown illustrated in Figure 12. The heat source follows the path of the part on the solid substrate. The element activation occurs when 5% of the maximum value of the heat flux is felt at a particular element at any time step.

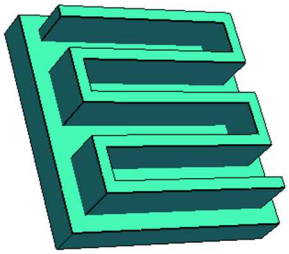

Figure 12: CASE STUDY : PART WITH THE SUBSTRATE.

The part with substrate was meshed with 25000 elements, and, at the beginning of the AM simulation, the elements above the substrate were turned 'off'. The bottom surface of the substrate was fixed at 298K, and top surface of the substrate and all surfaces of the final part are subject to both convection and radiation with heat transfer coefficient h = 35 W/m^{2}K, emissivity = 0.6, with ambient medium temperature at 298K.

The path is divided into 97 steps, and the coordinates are stored in a file. The laser is assumed to move at 0.1s per time step, corresponding to a laser speed of 5 mm/s. The volumetric heat flux given by Equation (2.11) is applied based on the location on the substrate at each time step. The temperature distribution at three different instances is illustrated in Figure 13. The entire transient thermal simulation of one layer of material was completed in 129 seconds.

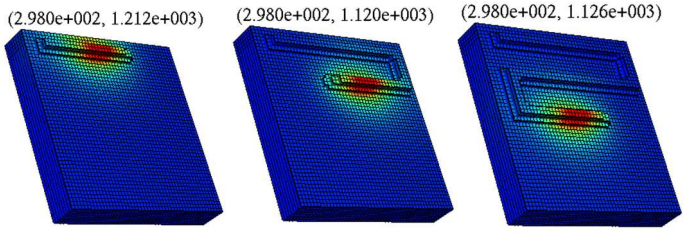

Figure 13: TEMPERATURE DISTRIBUTION at 0.8 S, 2.7 S, 4.8 S.

The finite element mesh after one layer of material deposition is illustrated in Figure 14. The cycle can be repeated for each layer, with no degradation in performance.

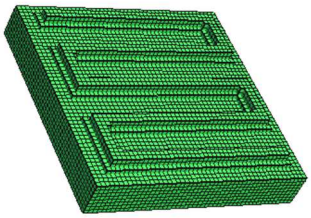

Figure 14: THE FIRST LAYER OF MATERIAL.

CONCLUSION

As a first step towards a fast simulation framework for additive manufacturing, this paper demonstrates an assembly-free transient thermal analysis with material deposition. As the experiments demonstrate, the method is sufficiently accurate (to within 0.15% of commercial implementations), but significantly faster (with a speed-up ranging from 2 to 50). Future work will focus on including phase change and fluid flow.

REFERENCES

[1] R. Martukanitz, P. Michaleris, T. Palmer, T. DebRoy, Z.-K. Liu, R. Otis, T. W. Heo, and L.-Q. Chen, "Toward an integrated computational system for describing the additive manufacturing process for metallic materials," *Addit. Manuf.*, vol. 1–4, pp. 52–63, Oct. 2014.

[2] I. Gibson, D. W. Rosen, and B. Stucker, *Additive Manufacturing Technologies*. Springer, 2010.

[3] F42 Committee, "Terminology for Additive Manufacturing Technologies," ASTM International, 2012.

[4] B. P. Conner, G. P. Manogharan, A. N. Martof, L. M. Rodomsky, C. M. Rodomsky, D. C. Jordan, and J. W. Limperos, "Making sense of 3-D printing: Creating a map of additive manufacturing products and services," *Addit. Manuf.*, vol. 1–4, pp. 64–76, Oct. 2014.

[5] P. Witherell, S. Feng, T. W. Simpson, D. B. Saint John, P. Michaleris, Z.-K. Liu, L.-Q. Chen, and R. Martukanitz, "Toward Metamodels for Composable and Reusable Additive Manufacturing Process Models," *J. Manuf. Sci. Eng.*, vol. 136, no. 6, pp. 061025–061025, Oct. 2014.

[6] K. V. Wong and A. Hernandez, "A Review of Additive Manufacturing," *ISRN Mech. Eng.*, vol. Article ID 208760, 2012.

[7] T. J. Horn and O. L. Harrysson, "Overview of current additive manufacturing technologies and selected applications," *Sci Prog*, vol. 95, no. 3, pp. 255–282, 2012.

[8] O. Marketing, "Metal 3d Printing Materials," *Optomec Additive Manufacturing*, 26-Jan-2015. .

[9] J. Goldak, A. Chakravarti, and M. Bibby, "A new finite element model for welding heat sources," *Metall. Trans. B*, vol. 15, no. 2, pp. 299–305, Jun. 1984.

[10] R. Ye, J. E. Smugeresky, B. Zheng, Y. Zhou, and E. J. Lavernia, "Numerical modeling of the thermal behavior during the LENS® process," *Mater. Sci. Eng. A*, vol. 428, no. 1–2, pp. 47–53, Jul. 2006.

[11] J. G. Michopoulos, S. Lambrakos, and A. Illopoulos, "Multiphysics Challenges for Controlling Layered Manufacturing Processes Targeting Thermomechanical Performance," *ASME*, vol. 1A.

[12] V. R. Voller, "An overview of numerical methods for solving phase change problems," in *Advances in Numerical Heat Transfer*, vol. 1, CRC Press, 1996.

[13] H. Hu and A. Argyropoulos, "Mathematical modelling of solidification and melting: a review," *Model. Simul Mater Sci Eng*, vol. 4, pp. 371–396, 1996.

[14] J. C. Heigel, P. Michaleris, and E. W. Reutzel, "Thermo-mechanical model development and validation of directed energy deposition additive manufacturing of Ti–6Al–4V," *Addit. Manuf.*, Jan. 2015.

[15] J. N. Reddy, *The finite element method in heat transfer and fluid dynamics*, 2nd ed. Boca Raton, FL: CRC Press, 2001.

[16] P. Michaleris, "Modeling metal deposition in heat transfer analyses of additive manufacturing processes," *Finite Elem. Anal. Des.*, vol. 86, pp. 51–60, Sep. 2014.

[17] R. D. Cook, D. S. Malkus, M. E. Plesha, and R. Witt, *Concepts and Applications of Finite Element Analysis*, 4th ed. John Wiley & Sons, 2002.

[18] S. Park, D. W. Rosen, S. Choi, and C. E. Duty, "Effective Mechanical Properties of Lattice Material Fabricated by Mateial Extrusion Additive Manufacturing," in *Proceedings of the ASME 2014 International Design Engineering Technical Conferences & Computers and Information in Engineering Conference*, Buffalo, NY, USA.

[19] T. J. R. Hughes, I. Levit, and J. Winget, "An element-by-element solution algorithm for problems of structural and solid mechanics," *Comput Meth Appl Mech Eng*, vol. 36, no. 2, pp. 241–254, 1983.

[20] P. Yadav and K. Suresh, "Limited-Memory Deflated Conjugate Gradient for Solid Mechanics," in *Proceedings of the ASME 2014 International Design Engineering Technical Conferences & Computers and Information in Engineering Conference*, Buffalo, NY, USA, 2014.

[21] P. Yadav and K. Suresh, "Large Scale Finite Element Analysis Via Assembly-Free Deflated Conjugate Gradient," *J Comput Inf Sci Eng*, vol. 14, no. 4, pp. 041008–1: 041008–9, 2014.

[22] J. N. Reddy, *An introduction to nonlinear finite element analysis*. Oxford University Press, 2004.